J|A|C|S
A R T I C L E S

Dynamics of a Myoglobin Mutant Enzyme: 2D IR Vibrational Echo Experiments and Simulations

Sayan Bagchi,[†] Benjamin T. Nebgen,[‡] Roger F. Loring,[‡] and M. D. Fayer*,[†]

Department of Chemistry, Stanford University, Stanford, California 94305, United States, and Department of Chemistry and Chemical Biology, Cornell University, Ithaca, New York 14853, United States

Abstract: Myoglobin (Mb) double mutant T67R/S92D displays peroxidase enzymatic activity in contrast to the wild type protein. The CO adduct of T67R/S92D shows two CO absorption bands corresponding to the A_1 and A_3 substates. The equilibrium protein dynamics for the two distinct substates of the Mb double mutant are investigated by using two-dimensional infrared (2D IR) vibrational echo spectroscopy and molecular dynamics (MD) simulations. The time-dependent changes in the 2D IR vibrational echo line shapes for both of the substates are analyzed using the center line slope (CLS) method to obtain the frequency-frequency correlation function (FFCF). The results for the double mutant are compared to those from the wild type Mb. The experimentally determined FFCF is compared to the FFCF obtained from molecular dynamics simulations, thereby testing the capacity of a force field to determine the amplitudes and time scales of protein structural fluctuations on fast time scales. The results provide insights into the nature of the energy landscape around the free energy minimum of the folded protein structure.

I. Introduction

The biological functions of proteins are intimately linked to their capacity to undergo structural changes. Protein dynamics, occurring on a wide range of time scales ranging from subpicosecond to milliseconds, have been the focus of both experimental and theoretical studies over recent years. Understanding protein dynamics can provide valuable insights into the relationships between protein structure and function.[1–5] Most biological processes occur on the electronic ground state potential energy surface. Therefore, it is useful to study protein dynamics in the ground electronic state that reflect thermal motions of the mechanical degrees of freedom. 2D IR vibrational echo spectroscopy,[6,7] which is an ultrafast IR analog of 2D NMR, provides sufficient temporal resolution to probe the fast motions of proteins on time scales from ~100 fs to ~100 ps. Fundamental structural sampling in this time range can bring an enzymatic system to its transition state as well as representing the initial stages of much slower structural evolution. Interpreting such measurements in terms of particular molecular motions requires theoretical treatment of the experimental observables in atomistic detail. The combination of complementary spec-

troscopic and computational studies can provide a detailed and self-consistent picture of protein structure, dynamics, and function.[8–12]

Carbonmonoxymyoglobin (MbCO) has been extensively studied both experimentally[13–26] and computationally.[27–33] The CO stretching mode of MbCO has a strong transition dipole,

† Stanford University.
‡ Cornell University.
(1) Campbell, B.; Chance, M.; Friedman, J. *Science* **1987**, *238*, 373.
(2) Hong, M. K.; Braunstein, D.; Cowen, B. R.; Frauenfelder, H.; Iben, I. E.; Mourant, J. R.; Ormos, P.; Scholl, R.; Schulte, A.; Steinbach, P. J. *Biophys. J.* **1990**, *58*, 429.
(3) Frauenfelder, H.; Sligar, S.; Wolynes, P. *Science* **1991**, *254*, 1598.
(4) Frauenfelder, H.; McMahon, B. H.; Austin, R. H.; Chu, K.; Groves, J. T. *Proc. Natl. Acad. Sci. U.S.A.* **2001**, *98*, 2370.
(5) Andrews, B. K.; Romo, T.; Clarage, J. B.; Pettitt, B. M.; Phillips, G. N. *Structure* **1998**, *6*, 587.
(6) Park, S.; Kwak, K.; Fayer, M. *Laser Phys. Lett.* **2007**, *4*, 704.
(7) Asbury, J. B.; Steinel, T.; Stromberg, C.; Gaffney, K. J.; Piletic, I. R.; Goun, A.; Fayer, M. D. *Chem. Phys. Lett.* **2003**, *374*, 362.

(8) Hummer, G.; Schotte, F.; Anfinrud, P. A. *Proc. Natl. Acad. Sci. U.S.A.* **2004**, *101*, 15330.
(9) Merchant, K. A.; Noid, W. G.; Akiyama, R.; Finkelstein, I. J.; Goun, A.; McClain, B. L.; Loring, R. F.; Fayer, M. D. *J. Am. Chem. Soc.* **2003**, *125*, 13804.
(10) Merchant, K. A.; Thompson, D. E.; Xu, Q.-H.; Williams, R. B.; Loring, R. F.; Fayer, M. D. *Biophys. J.* **2002**, *82*, 3277.
(11) Merchant, K. A. Ph.D. Dissertation, Stanford University, 2003.
(12) Williams, R. B.; Loring, R. F.; Fayer, M. D. *J. Phys. Chem.* **2001**, *105*, 4068.
(13) Springer, B. A.; Sligar, S. G.; Olson, J. S.; Phillips, G. N., Jr. *Chem. Rev.* **1994**, *94*, 699.
(14) Rector, K. D.; Engholm, J. R.; Rella, C. W.; Hill, J. R.; Dlott, D. D.; Fayer, M. D. *J. Phys. Chem. A* **1999**, *103*, 2381.
(15) Caughey, W. S.; Shimada, H.; Choc, M. G.; Tucker, M. P. *Proc. Natl. Acad. Sci. U.S.A.* **1981**, *78*, 2903.
(16) Tian, W. D.; Sage, J. T.; Champion, P. M.; Chien, E.; Sligar, S. G. *Biochem.* **1996**, *35*, 3487.
(17) Zhu, L.; Sage, J. T.; Rigos, A. A.; Morikis, D.; Champion, P. M. *J. Mol. Biol.* **1992**, *224*, 207.
(18) Shimada, H.; Caughey, W. S. *J. Biol. Chem.* **1982**, *257*, 11893.
(19) Johnson, J. B.; Lamb, D. C.; Frauenfelder, H.; Müller, J. D.; McMahon, B.; Nienhaus, G. U.; Young, R. D. *Biophys. J.* **1996**, *71*, 1563.
(20) Muller, J. D.; McMahon, B. H.; Chien, E. Y. T.; Sligar, S. G.; Ulrich Nienhaus, G. *Biophys. J.* **1999**, *77*, 1036.
(21) Phillips, G. N.; Teodoro, M. L.; Li, T.; Smith, B.; Olson, J. S. *J. Phys. Chem. B* **1999**, *103*, 8817.
(22) Fayer, M. D. *Annu. Rev. Phys. Chem.* **2001**, *52*, 315.
(23) Morikis, D.; Champion, P. M.; Springer, B. A.; Sligar, S. G. *Biochemistry* **1989**, *28*, 4791.
(24) Nienhaus, G. U.; Mourant, J. R.; Chu, K.; Frauenfelder, H. *Biochemistry* **1994**, *33*, 13413.
(25) Oldfield, E.; Guo, K.; Augspurger, J. D.; Dykstra, C. E. *J. Am. Chem. Soc.* **1991**, *113*, 7537.

making its infrared absorption a readily monitored experimental observable to track protein vibrational dynamics. Studies on myoglobin (Mb), and in particular on MbCO, serve as tests for many of the ideas on the relationship between structure and function in proteins.[34] Because of the relatively small size of Mb, molecular dynamics (MD) simulations over the time scales relevant to vibrational echo spectroscopy are readily performed,[28,29] permitting a direct comparison between simulations and experiments. Much of the detailed understanding of Mb and its conformational dynamics has come from a combination of simulations and biophysical studies on the native protein and a library of mutants with several key residues modified.[23,35−37]

Wild type Mb can adopt several different conformational substates at room temperature.[15,38] The spectroscopic signature of the structural substates is the multiple peak linear absorption spectrum of the heme-ligated CO stretching mode of Mb,[5,39,40] which is dominated by three bands corresponding to the substates labeled A_0, A_1, and A_3. Structural differences among these substates involve the conformation of the imidazole side chain on the distal histidine His 64. At low pH, the A_0 band dominates the spectrum and is believed to be associated with a doubly protonated His 64 imidazole that is rotated out of the heme pocket away from the heme-ligated CO.[41] Above pH of 6.0, the A_1 and A_3 bands dominate the spectrum.

That significant structural changes occur in the $A_1−A_3$ interconversion is supported by X-ray experiments. The high resolution crystal structure of MbCO that contains two conformations has enabled modeling of the structure of A_1 and A_3 substates.[42] Although the distal histidine has a critical role in determining the substates of Mb, structural comparison between the A_1 and A_3 substates shows that the A_3 substate contains an additional cavity, Xe3, and another transient cavity found in simulations.[42] Xe is used as a probe to identify the locations of cavities in proteins.[43,44] In Mb crystals, four Xe atoms (Xe1, Xe2, Xe3, and Xe4) occupy cavities, which may be involved in gas ligand migration.[42,43] The Xe3 site, which is near the

surface and far from the iron atom, involves Trp-7 and is located between helices E and H.[43] The existence of Xe3 in the A_3 substate but not in the A_1 substate demonstrates that the difference in the substates is significant.

Comparison of measured and simulated absorption spectra and infrared vibrational echoes of wild-type Mb have indicated that an important structural difference between A_1 and A_3 substates is a rotation of the singly protonated imidazole of His 64.[9,10,12] Devereux and Meuwly[45] have used electronic structure methods combined with molecular dynamics simulations using the CHARMM force field to investigate spectroscopic substates of wild-type Mb. Their calculations do not support our interpretation of the structures associated with the A_1 and A_3 substates in wild-type Mb, but also do not produce any candidate structures consistent with the experimentally observed dominant A_1 substate.

Peroxidases catalyze the oxidation of a wide range of substrates by hydrogen peroxide. The reaction with hydrogen peroxide is facilitated by a "push-pull" mechanism, with a significant contribution from the suitably positioned residues located in both heme proximal and distal sites. Myoglobin shares the same heme cofactor and the same heme distal and proximal His residues (His 64 and His 93)[46] with typical peroxidase enzymes.[47] However the differences in heme environment and overall polarity of the active site make the catalytic activity of Mb virtually negligible compared to peroxidases. It has been shown that site-directed mutagenesis, used to introduce a distal arginine and a proximal aspartate (T67R/S92D) (see Figure 1), enhances the peroxidase activity of Mb,[48,49] making the double mutant a very interesting system to study and compare with the wild type variant. The distal histidine and arginine favor the O−O bond polarization of the Fe-bound hydrogen peroxide, whereas the proximal aspartate weakens the peroxide O−O bond by increasing the electron-donating character of the proximal histidine through a hydrogen bond to the imidazole NH group.

In this study, we report measurements of the fast equilibrium structural dynamics of the two distinct conformational substates (A_1 and A_3) of the double mutant of Mb (T67R/S92D). The experimental measurements are made using 2D IR vibrational echo spectroscopy. The frequency-frequency correlation function (FFCF), which connects the experimental observables to the underlying protein structural dynamics, is extracted from the waiting time dependence of the 2D spectra using the center line slope (CLS) method.[6,50] Comparisons of the dynamics of the Mb double mutant (Figure 1A) with that of wild type Mb (Figure 1B) are also presented.[9,10,12,51−53] The structural dynamics of the double mutant are studied in MD simulations. Using the MD simulation results, the FFCFs for both substates are

(26) Ansari, A.; Berendzen, J.; Braunstein, D.; Cowen, B. R.; Frauenfelder, H.; Hong, M. K.; Iben, I. E. T.; Johnson, J. B.; Ormos, P.; Sauke, T. B.; Scholl, R.; Schulte, A.; Steinbach, P. J.; Vittitow, J.; Young, R. D. *Biophys. Chem.* **1987**, *26*, 337.
(27) Rovira, C.; Schulze, B.; Eichinger, M.; Evanseck, J. D.; Parrinello, M. *Biophys. J.* **2001**, *81*, 435.
(28) Schulze, B. G.; Evanseck, J. D. *J. Am. Chem. Soc.* **1999**, *121*, 6444.
(29) Meller, J.; Elber, R. *Biophys. J.* **1998**, *74*, 789.
(30) Elber, R.; Karplus, M. *Science* **1987**, *235*, 318.
(31) Kushkuley, B.; Stavrov, S. S. *Biophys. J.* **1996**, *70*, 1214.
(32) Kushkuley, B.; Stavrov, S. S. *Biophys. J.* **1997**, *72*, 899.
(33) Vitkup, D.; Ringe, D.; Petsko, G. A.; Karplus, M. *Nat. Struct. Biol.* **2000**, *7*, 34.
(34) Frauenfelder, H.; McMahon, B. H.; Fenimore, P. W. *Proc. Natl. Acad. Sci. U.S.A.* **2003**, *100*, 8615.
(35) Henry, E. R.; Sommer, J. H.; Hofrichter, J.; Eaton, W. A.; Gellert, M. *J. Mol. Biol.* **1983**, *166*, 443.
(36) Martin, J.-L.; Vos, M. H. In *Methods in Enzymology*; Everse, J., Vandergriff, K. D., Winslow, R. M., Eds.; Academic Press: New York, 1994; Vol. 232, p 416.
(37) Balasubramanian, S.; Lambright, D. G.; Simmons, J. H.; Gill, S. J.; Boxer, S. G. *Biochemistry* **1994**, *33*, 8355.
(38) Makinen, M. W.; Houtchens, R. A.; Caughey, W. S. *Proc. Natl. Acad. Sci. U.S.A.* **1979**, *76*, 6042.
(39) Li, T.; Quillin, M. L.; Phillips, G. N.; Olson, J. S. *Biochemistry* **1994**, *33*, 1433.
(40) Anderton, C. L.; Hester, R. E.; Moore, J. N. *Biochim. Biophys. Acta, Protein Struct. Mol. Enzymol.* **1997**, *1338*, 107.
(41) Yang, F.; Phillips, G. N. *J. Mol. Biol.* **1996**, *256*, 762.
(42) Teeter, M. M. *Protein Sci.* **2004**, *13*, 313.
(43) Tilton, R. F.; Kuntz, I. D.; Petsko, G. A. *Biochemistry* **1984**, *23*, 2849.
(44) Doukov, T. I.; Blasiak, L. C.; Seravalli, J.; Ragsdale, S. W.; Drennan, C. L. *Biochemistry* **2008**, *47*, 3474.

(45) Devereux, M.; Meuwly, M. *Biophys. J.* **2009**, *96*, 4363.
(46) Antonini, E.; Brunori, M. *Hemoglobin and Myoglobin in Their Reactions with Ligands*; North Holland Publishing Co.: Holland, 1971.
(47) Gajhede, M.; Schuller, D. J.; Henriksen, A.; Smith, A. T.; Poulos, T. L. *Nat. Struct. Biol.* **1997**, *4*, 1032.
(48) Roncone, R.; Monzani, E.; Nicolis, S.; Casella, L. *Eur. J. Inorg. Chem.* **2004**, *2203*.
(49) Roncone, R.; Monzani, E.; Murtas, M.; Battaini, G.; Pennati, A.; Sanangelanton, A. M.; Zuccotti, S.; Bolognesi, M.; Casella, L. *Biochem. J.* **2004**, *377*, 717.
(50) Kwak, K.; Park, S.; Finkelstein, I. J.; Fayer, M. D. *J. Chem. Phys.* **2007**, *127*, 124503.
(51) Rella, C. W.; Kwok, A. S.; Rector, K. D.; Hill, J. R.; Schwettman, H. A.; Dlott, D. D.; Fayer, M. D. *Phys. Rev. Lett.* **1996**, *77*, 1648.
(52) Rella, C. W.; Rector, K. D.; Kwok, A.; Hill, J. R.; Schwettman, H. A.; Dlott, D. D.; Fayer, M. D. *J. Phys. Chem.* **1996**, *100*, 15620.
(53) Merchant, K. A.; Noid, W. G.; Thompson, D. E.; Akiyama, R.; Loring, R. F.; Fayer, M. D. *J. Phys. Chem. B* **2003**, *107*, 4.
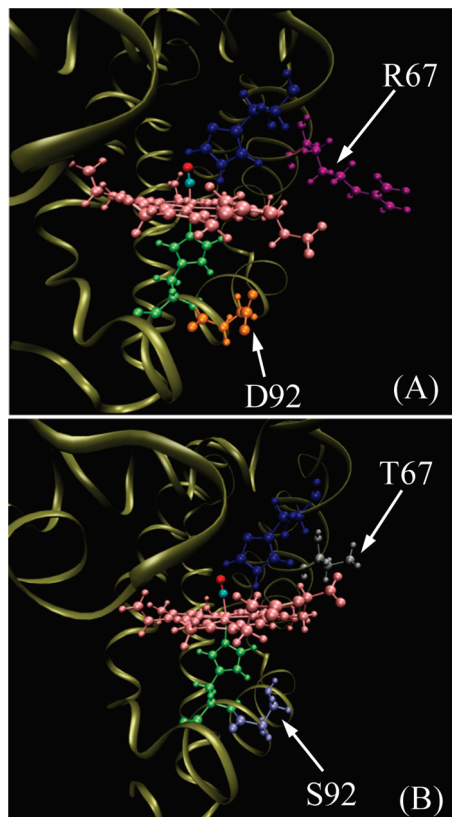
Figure 1. Structures of CO bound (A) T67R/S92D double mutant and (B) wild type myoglobin. Arg 67 and Asp 92 (for T67R/S92D), Thr 67 and Ser 92 (for wild type Mb) are indicated.

calculated with the method applied previously to wild type and mutant Mb.[9,10,12,53] The results of the MD simulations are compared with the experimentally determined FFCFs. The simulated FFCFs reflect the fast structural fluctuations of the protein that are predicted by the force field used for the molecular dynamics. The accuracy and applicability of the empirical force fields applied to biomolecules are conventionally assessed using structural criteria.[54] The comparison of simulated and measured FFCFs provides an uncommon opportunity to test the capacity of a force field to reproduce the time scales of rapid conformational changes in proteins.

The amplitudes and time scales of the protein structural dynamics obtained from experiments agree well with the simulation results. The results provide insights into the nature of the energy landscape around the free energy minimum of the folded protein structure.

II. Materials, Methods, and Procedures

A. Samples. The Mb double mutant (T67R/S92D) plasmid was obtained from Professor Luigi Casella, Dipartimento di Chimia Generale, University of Pavia, Italy. The original plasmid was modified such that it contains an N-terminal His-tag with an adjacent thrombin cleavage site. This was necessary because the mutant with the His-tag aggregated at concentrations too low to perform the experiments. The Mb mutant was expressed in the *Escherichia coli* BL21(DE3) strain. The cells were grown to a density of $A_{600} = 0.6$ when the protein expression was induced with 1 mM IPTG. After overnight growth at 18 °C, the cells were harvested by

centrifugation at 4 °C for 30 min at 6000 rpm. The dark-brown bacterial pellet containing the Mb mutant was resuspended in lysis buffer (100 mM HEPES/300 mM NaCl/20% glycerol, pH 7.0), containing 0.5 mM dithiothreitol and 1 mM PMSF (protease inhibitor), and lysed by sonication. The crude lysate was centrifuged, filtered and loaded onto a Ni-NTA column. The His-tagged protein was eluted by HEPES/300 mM NaCl/20% glycerol/200 mM imidazole and was desalted into His-tag cleavage buffer (20 mM Tris/150 mM NaCl/2.5 mM CaCl$_2$, pH 7.5). To remove the His-tag, thrombin was added to the solution and left overnight, followed by another buffer exchange to 50 mM MES/1 mM EDTA/0.5 mM DTT and loaded on to a CM-FF cation-exchange column. Fractions containing the Mb double mutant were collected and the purity was checked by monitoring the absorbance ratio A_{Soret}/A_{280}, which was above 3.5.

The Mb solution was reduced with excess dithionite solution and stirred under a CO atmosphere for an hour before being filtered with a 0.45 μm filter. The final concentration and pH of the Mb mutant used for the 2D IR vibrational echo experiments were ~3 mM and 6.0 respectively. Though the pH of the MbCO (wild type) solutions used in previous 2D-IR vibrational echo experiments was 7.0, the double mutant was found to be most stable at pH 6.0. Therefore, the experiments on wild type MbCO were performed at both pH 6.0 and 7.0. The previous vibrational echo studies[9,10,12] of wild type MbCO were not heterodyne detected (see Sec. IIB below). Repeating the experiments with the current heterodyne detected method allowed for a better comparison as the double mutant and wild type data were taken on the same instrument using the same methodology.

B. 2D IR Vibrational Echo Experiment. In a 2D IR vibrational echo experiment, three ultrashort IR pulses tuned to span the vibrational absorption frequencies of A$_1$ and A$_3$ are crossed in the sample. The IR excitation pulses, (110 fs in duration and 150 cm^{-1} fwhm) are produced using a Ti:Sapphire regenerative amplifier pumped optical parametric amplifier system.[55] The broad bandwidth of these ultrashort pulses makes it possible to simultaneously excite the CO stretching vibration of both the A$_1$ and A$_3$ substates. The three successive ultrashort IR pulses with wave vectors $\vec{k}_1$, $\vec{k}_2$, and $\vec{k}_3$ are applied to the sample to induce the subsequent emission of the vibrational echo. The vibrational echo signal in the phase matching direction (wave vector $\vec{k}_s = -\vec{k}_1 + \vec{k}_2 + \vec{k}_3$) is detected, with frequency and phase resolution, by combining it with a local oscillator (LO) pulse. The combined pulses are dispersed in a monochromator and then detected with a 32-element MCT IR array detector, which measures the signal at 32 wavelengths simultaneously.

2D IR vibrational echo data is a function of three variables: the emitted vibrational echo frequency (ω_m), the variable time delay between the first and second pulses (τ), and the variable time separation between the second and third pulses (T_w or the waiting time). Numerical Fourier transforms of the temporal interferograms that result from the τ scan at each frequency ω_m gives the second frequency variable, ω_τ. The results are plotted as a two-dimensional spectrum with frequency variables ω_τ and ω_m. A 2D spectrum is obtained for each waiting time, T_w.

The interaction of the protein sample with the three ultrashort pulses in a 2D IR vibrational echo experiment can be viewed qualitatively as follows. The first IR pulse excites the molecules to a coherent superposition of two vibrational states which causes the molecules to oscillate in phase with their initial frequencies. The second IR pulse transfers this coherence into a population. The structural evolution of the proteins during the population period causes the initially labeled frequencies to change (spectral diffusion), which contributes to the 2D line shapes. Thus, increasing T_w gives more time for the structural evolution of proteins, thereby changing the shape of the 2D spectral bands. The interaction of the third pulse ends the evolution period and brings the molecules to a second coherence. During the second coherence period, the final frequencies

(54) Hornak, V.; Abel, R.; Okur, A.; Strockbine, B.; Roitberg, A.; Simmerling, C. *Proteins* **2006**, *65*, 712.

(55) Asbury, J. B.; Steinel, T.; Fayer, M. D. *J. Lumin.* **2004**, *107*, 271.

of the frequency-labeled molecules are read out by the vibrational echo pulse. A 2D correlation map (spectrum) is obtained with the initial labeled frequencies (ω_τ) as one axis in the 2D spectrum and the final frequencies (ω_m) of the molecules as the other axis. By analyzing the amplitudes, positions, and peak shapes of the 2D spectra, detailed information on structure and dynamics of the molecular system is obtained.

The changes in the line shapes of the 2D bands with increasing waiting time can be used to obtain the time scales and amplitudes of the various contributions to the structural dynamics of the proteins within the experimental time window (~100 ps), which is limited by the CO vibrational lifetime. From the T_w dependence of the 2D spectra, the FFCF is obtained. The FFCF quantifies the correlation between an initial value of the vibrational frequency of the CO stretch and the value of this frequency at a later time. The frequency evolution is caused by structural evolution of the protein. The center line slope (CLS) method[6,50] is used to extract the FFCF from the T_w dependent 2D spectra. The CLS analysis combined with the linear absorption spectrum gives the full FFCF, including any T_w independent homogeneous component.

C. Molecular Dynamics Simulation. One molecule of the mutant Mb T67R/S92D with CO bound was simulated in a solvent of 3858 SPC/E water molecules[56,57] with periodic boundary conditions using the Amber 10 simulation package with the 2003 force field.[58−60] The calculations were performed at constant temperature, $T = 300$ K. The carbonmonoxy T67R/S92D molecule was constructed from the structure 1H1X[49] in the Protein Data Bank[61] by replacing the CN^- ligand with CO, by adding protons including the protonation of the N_ε on the distal histidine H64,[9] and by removing a sulfate ion and adding a chloride ion to preserve electroneutrality. Since the Fe−C−O unit is nearly linear in Mb, we have introduced force parameters of value zero for the N−Fe−C−O dihedral angles to null the torque on these angles. Two partial charge models[45] were employed for the CO ligand; in the first model the charges were assigned gas phase[45] values $\pm 0.021e$ as used in the MOIL force field employed in previous simulations[9,62−64] of MbCO, and in the second model the charges were $\pm 0.17e$ as calculated for carbonmonoxyneuroglobin by Anselmi, et al.[65] As described below, the simulated protein fluctuated between two sets of conformational states,[9] which we assign to the A_1 and A_3 spectroscopic substates. For each model of CO partial charges and starting in each substate, eight distinct trajectories of length 2 ns were obtained.

Spectroscopic observables are linked to molecular dynamics trajectories through the electrostatic model employed in previous studies of wild-type Mb,[9] the mutant Mb H64V,[62−64] and horseradish peroxidase.[66] In this classical mechanical picture, the local electric force at the ligand induces an instantaneous frequency shift in the CO vibrational frequency which therefore fluctuates in time with the force. This frequency fluctuation is given by

$$\delta\omega(t) = \lambda[\vec{u}(t)\cdot\vec{E}(t) - \langle\vec{u}\cdot\vec{E}\rangle] \tag{1}$$

The electric field $\vec{E}(t)$ is determined at the midpoint of the CO bond from molecular dynamics trajectories, the partial charges in the Amber force field, and Coulomb's law in vacuum. In eq 1, $\vec{u}$ is a unit vector pointing along the CO bond and the angle brackets denote an equilibrium average. The parameter λ plays the role of a microscopic version of the Stark effect tuning rate. The macroscopic vibrational Stark effect tuning rate has been measured for heme proteins including Mb by Park, et al.[67−69] to be in the range $\lambda = 1.8−2.2$ cm^{-1}/(MV/cm). Previous calculations of vibrational echoes and infrared lineshapes from molecular dynamics simulations of wild-type Mb and the mutant Mb H64V employed the MOIL force field.[70] With this force field, the spectroscopic observables were consistent with $\lambda = 2.1$ cm^{-1}/(MV/cm), which lies in the experimental range of values. With the different atomic partial charges of the Amber force field, we have found that a smaller value of $\lambda \approx 1$ cm^{-1}/(MV/cm) is required to reproduce linear and nonlinear spectra for wild type Mb,[66] horseradish peroxidase[66] and T67R/S92D. In the present study, the value of $\lambda = 1.0$ cm^{-1}/(MV/cm) is employed in all calculations presented below. The value of λ needed in eq 1 to convert a local, microscopic electric field to a vibrational frequency shift need not be quantitatively comparable to the macroscopic Stark tuning rate determined in a bulk measurement, because of local field effects. The equilibrium autocorrelation function of frequency fluctuations (FFCF),

$$C(t) = \langle\delta\omega(t)\,\delta\omega(0)\rangle \tag{2}$$

is then computed from eq 1 by averaging over trajectories and is used to calculate spectroscopic observables through a standard cumulant approximation that is valid in the limit of weak coupling between the CO vibrational coordinate and its environment.[53,71] The MD simulations are independent of λ, which is used to convert simulated electric fields to spectroscopic frequencies. As the frequency fluctuation in eq 1 is linear in λ, the FFCF in eq 2 is quadratic in λ, so that varying λ corresponds to changing the overall amplitude of $C(t)$, leaving its decay times unchanged.

As shown in Figure 5 below, trajectories of $\delta\omega(t)$ in eq 1 simulated for T67R/S92D show clear two-state switching behavior, as observed previously in simulations of wild-type Mb.[53,71] We assign these two frequency states to the A_1 and A_3 spectroscopic substates. The cumulant approximation on which our spectroscopic calculations are based rests on an assumption of Gaussian frequency fluctuations, which would be an inappropriate description of two-state dynamics. Because of the separation of time scales between fluctuations within a substate and switching between substates, we treat the substate interconversion in a static limit. We compute separate FFCFs for the two substates, which amounts to the reasonable assumption that frequency fluctuations within each substate may be treated as Gaussian, even though the switching dynamics may not be so treated. The distinction between the two states is sufficiently clear that identifying these states is not ambiguous, as can be seen in Figure 5 below. After a given trajectory is divided into A_1 and A_3 segments, 50 ps of frequency trajectory is removed on each side of an identified transition. Any

(56) Berendsen, H. J. C.; Grigera, J. R.; Straatsma, T. P. *J. Phys. Chem.* **1987**, *91*, 6269.
(57) van der Spoel, D.; van Maaren, P. J.; Berendsen, H. J. C. *J. Chem. Phys.* **1998**, *108*, 10220.
(58) Case, D. A.; et al. *AMBER 10*; University of California: San Francisco, 2008.
(59) Giammona, D. A. Ph.D. Dissertation, University of California, Davis, 1984.
(60) Duan, Y.; Wu, C.; Chowdhury, S.; Lee, M. C.; Xiong, G.; Zhang, W.; Yang, R.; Cieplak, P.; Luo, R.; Lee, T.; Caldwell, J.; Wang, J.; Kollman, P. *J. Comput. Chem.* **2003**, *24*, 1999.
(61) Berman, H. M.; Westbrook, J.; Feng, Z.; Gilliland, G.; Bhat, T. N.; Weissig, H.; Shindyalov, I. N.; Bourne, P. E. *Nucleic Acids Res.* **2000**, *28*, 235.
(62) Finkelstein, I. J.; Goj, A.; McClain, B. L.; Massari, A. M.; Merchant, K. A.; Loring, R. F.; Fayer, M. D. *J. Phys. Chem. B* **2005**, *109*, 16959.
(63) Massari, A. M.; Finkelstein, I. J.; McClain, B. L.; Goj, A.; Wen, X.; Bren, K. L.; Loring, R. F.; Fayer, M. D. *J. Am. Chem. Soc.* **2005**, *127*, 14279.
(64) Goj, A.; Loring, R. F. *Chem. Phys.* **2007**, *341*, 37.
(65) Anselmi, M.; Brunori, M.; Vallone, B.; Di Nola, A. *Biophys. J.* **2007**, *93*, 434.
(66) Gruenbaum, S. M. Ph.D. Dissertation, Cornell University, 2010.

(67) Park, E. S.; Andrews, S. S.; Hu, R. B.; Boxer, S. G. *J. Phys. Chem. B* **1999**, *103*, 9813.
(68) Park, E. S.; Boxer, S. G. *J. Phys. Chem. B* **2002**, *106*, 5800.
(69) Park, E. S.; Boxer, S. G. *J. Phys. Chem. B* **2002**, *106*, 8910.
(70) Elber, R.; Roitberg, A.; Simmerling, C.; Goldstein, R.; Li, H. Y.; Verkhivker, G.; Keasar, C.; Zhang, J.; Ulitsky, A. *Comput. Phys. Commun.* **1995**, *91*, 159.
(71) Merchant, K. A.; Noid, W. G.; Akiyama, R.; Finkelstein, I.; Goun, A.; McClain, B. L.; Loring, R. F.; Fayer, M. D. *J. Am. Chem. Soc.* **2003**, *125*, 13804.
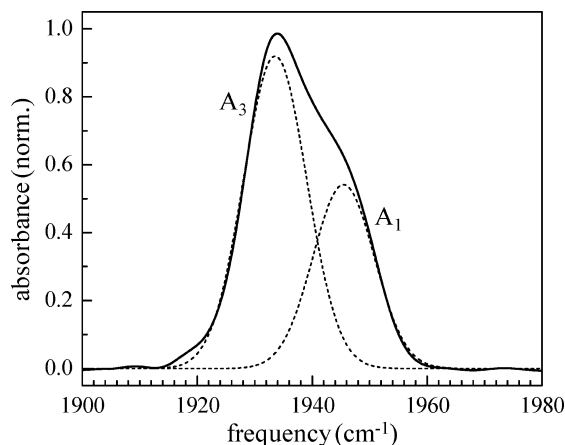
Figure 2. FT-IR spectrum of the CO stretch of heme-ligated CO for the myoglobin double mutant T67R/S92D (solid curve). The spectrum was fit with two Gaussians (dashed curves), representing the absorption bands of the A_1 and A_3 substates.

segment of duration less than 200 ps, an infrequent occurrence, is not included in the FFCF calculations. These distinct FFCFs are then used to compute linear and nonlinear spectra, which therefore include features associated with each substate but not the effects of substate interconversion.

III. Results and Discussion

A. Linear Absorption Spectroscopy. The FT-IR spectrum of wild type myoglobin at pH 6.0 shows three discrete CO stretching bands, labeled A_0, A_1, and A_3,[26,39,72] with identical peak positions as those at pH 7.0. The A_1 substate of wild type MbCO is predominantly populated in the absorption spectrum, and the A_0 band is very small. The background subtracted linear absorption spectrum of CO bound to the myoglobin double mutant (T67R/S92D) is displayed in Figure 2. The spectrum shows that MbCO (T67R/S92D) exists in at least two spectroscopically distinct conformational substates. In this spectrum the A_0 band, which is small in the wild type spectrum, cannot be seen. The spectrum is fit to two Gaussians, representing the absorption bands of the A_1 state at 1945 cm^{-1} and the A_3 state at 1932 cm^{-1}. The peak positions for the CO absorption bands of T67R/S92D obtained from fitting are essentially identical to those of the wild type Mb.[39] In contrast to wild type MbCO, the A_3 band of the double mutant is more intense than the A_1 band, which appears as the high frequency shoulder in the FT IR spectrum.

B. 2D IR Vibrational Echo Spectroscopy. Several 2D IR spectra of CO bound to Mb double mutant (T67R/S92D) are shown in Figure 3 at different waiting times (T_w). Each 2D spectrum has a pair of diagonal peaks (red, positive going) that correspond to the 0−1 CO stretch vibrational transition. Below the diagonal peaks are bands shifted along the vertical axis by the anharmonicity of the CO stretching mode (blue, negative going). These correspond to vibrational echo emission at the 1−2 transition frequency.[73,74] The peak centered at $(\omega_\tau, \omega_m) = (1932 \text{ cm}^{-1}, 1932 \text{ cm}^{-1})$ arises from the A_3 substate and that at $(1945 \text{ cm}^{-1}, 1945 \text{ cm}^{-1})$ from the A_1 substate. The peaks from

0−1 and 1−2 transitions decay with increased waiting time at a rate determined by the vibrational lifetime (T_1). Lifetimes of the individual substates were measured using IR pump−probe experiments. The lifetimes for the A_1 and the A_3 substates of the double mutant are 22 and 20 ps respectively.

As T_w increases, the shapes of the 2D peaks change, but the peak positions remain fixed. The highly elongated bands along the diagonal at short time become less elongated and increasingly symmetrical, which is a manifestation of spectral diffusion caused by the protein structural evolution. Detailed analysis of the waiting time dependence of the 2D line shapes quantifies the structural dynamics of the protein.

Cross peaks between the A_1 and A_3 substates in both the 0−1 and 1−2 regions of the 2D spectra grow in as the waiting time is increased. These cross peaks are the signature of conformational switching between A_1 and A_3 substates.[75] At longer T_w, substate interconversion has occurred to a non-negligible extent, which is manifested in the growth of cross peaks. Detailed analysis of conformational switching between the substates of the double mutant will be presented in another publication.[76] Because the substate conformational switching is so slow ($\sim$75 ps), the appearance of the off-diagonal peaks does not interfere with analysis of the time evolution of the shapes of the diagonal peaks, which gives the spectral diffusion.[77] To compare the dynamics of T67R/S92D with the wild type Mb, 2D IR spectra of wild type MbCO (sperm whale) were also measured at different values of T_w (spectra not shown). The 2D spectra mainly consist of the 0−1 and 1−2 peaks corresponding to the predominantly populated A_1 substate, with the 0−1 peak centered at $(\omega_\tau, \omega_m) = (1945 \text{ cm}^{-1}, 1945 \text{ cm}^{-1})$.

The FFCF connects the waiting time dependent changes in the 2D band shapes caused by spectral diffusion to the time dependence of the structural changes of the proteins. The CLS method is used here to determine the FFCF from 2D and linear spectra.[50,78] This method provides an accurate way to extract the FFCF and also provides a useful quantity to plot for visualizing differences in the protein dynamics for different substates and proteins.[50,78] It also facilitates the comparison of experimental data with simulations. At a particular ω_m, a slice through the 2D spectrum, projected onto the ω_τ axis, is a spectrum with a peak at a particular ω_τ value. Many such slices taken over a range of ω_m values produce a set of points. Connecting the resulting points yields the center line. At short T_w, the center line has a finite slope. In the absence of a homogeneous contribution, at $T_w = 0$, the 2D line shape is a line along the diagonal and the slope of the center line would be 1. At sufficiently long time, when spectral diffusion has sampled all frequencies, the 2D band is symmetrical; the center line is vertical with an infinite slope. It has been shown theoretically that the T_w-dependent part of the FFCF is directly related to the T_w dependence of the inverse of the slope of the center line.[50,78] Thus the inverse slope of the center line, which we will refer to as the CLS will vary between a maximum of 1 at $T_w = 0$ and 0 in the limit of long waiting time. The $T_w = 0$ slope will only be unity if there is no homogeneous

(72) Tian, W. D.; Sage, J. T.; Champion, P. M. *J. Mol. Biol.* **1993**, *233*, 155.

(73) Rector, K. D.; Kwok, A. S.; Ferrante, C.; Tokmakoff, A.; Rella, C. W.; Fayer, M. D. *J. Chem. Phys.* **1997**, *106*, 10027.

(74) Golonzka, O.; Khalil, M.; Demirdoven, N.; Tokmakoff, A. *Phys. Rev. Lett.* **2001**, *86*, 2154.

(75) Ishikawa, H.; Kwak, K.; Chung, J. K.; Kim, S.; Fayer, M. D. *Proc. Natl. Acad. Sci. U.S.A.* **2008**, *105*, 8619.

(76) Bagchi, S.; Thorpe, D. G.; Thorpe, I. F.; Voth, G. A.; Fayer, M. D. *J. Phys. Chem. B* [Online early access]. DOI: 10.1021/jp109203b. Published Online: Dec 3, 2010.

(77) Kwak, K.; Zheng, J.; Cang, H.; Fayer, M. D. *J. Phys. Chem. B* **2006**, *110*, 19998.

(78) Kwak, K.; Rosenfeld, D. E.; Fayer, M. D. *J. Chem. Phys.* **2008**, *128*, 204505.
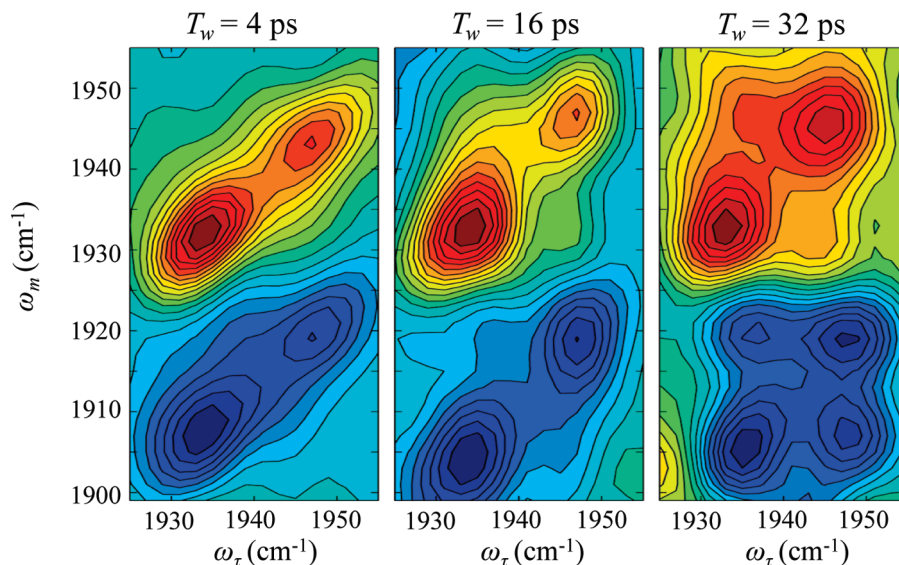
Figure 3. 2D IR spectra of CO bound to T67R/S92D at various waiting times T_w. The bands in the upper half of the spectrum (red) correspond to the $0-1$ vibrational transition. The bands in the lower half of the spectrum (blue) arise from the vibrational echo emission at the $1-2$ transition frequency.

contribution to the spectrum. The homogeneous contribution to the line shapes in the linear absorption and 2D spectra mainly comes from the motionally narrowed component produced by very fast structural fluctuations,[79−81] such that $\Delta\tau < 1$, where τ and Δ are the time constant and range (amplitude) of the frequency fluctuations. Other homogeneous contributions arise either from vibrational lifetime T_1, which is measured independently by IR pump−probe experiments, or from orientational relaxation, which can be neglected due to the large size, and therefore, very slow orientational relaxation of the protein. The homogeneous component of the spectrum causes the initial value of the inverse slope to be less than 1 at $T_w = 0$. The difference from 1 at $T_w = 0$ combined with the T_w dependent CLS and the linear absorption spectrum yields the full FFCF, including the T_w independent homogeneous component.[50,78]

The multiple time scale dynamics were modeled by a multiexponential form of the FFCF, $C(t)$.

$$C(t) = \sum_{i=1}^{n} \Delta_i^2 e^{-t/\tau_i} + \Delta_s^2 \qquad (3)$$

The Δ_i and τ_i terms are amplitudes and correlation times respectively, of the vibrational frequency fluctuations induced by protein structural dynamics. For the ith dynamical process, Δ_i is the range of CO frequencies sampled due to protein structural fluctuations, and τ_i is the time constant of these fluctuations. This form of the FFCF has been widely used and in particular found applicable in studies of the structural dynamics of heme-CO proteins.[9,10,62,79,82−86] The experimental

time window of several times T_1 is limited by the lifetime decay, which reduces the signal to zero. Occurrence of very slow structural fluctuations on time scales longer than the experimental time window, if present, will appear as the static term Δ_s^2 in the FFCF.

Δ_i and τ_i are obtained from the 2D data. However for a motionally narrowed term with $\Delta_i\tau_i < 1$, these quantities cannot be evaluated separately; only the product $\Delta^2\tau = 1/T_2$, can be determined. The pure dephasing component of the homogeneous dephasing time, T_2^*, is determined by using $(1)/(T_2) = (1)/(T_2^*) + (1)/(2T_1)$, where T_2 is obtained from the CLS with use of the linear absorption spectrum and T_1, the vibrational lifetime, is obtained from IR pump−probe experiments. The pure dephasing homogeneous line width is $\Gamma = 1/\pi T_2^*$.

Figure 4 shows the T_w dependent CLS data for the A_1 and A_3 bands of the CO bound Mb double mutant T67R/S92D. The points are derived from 2D IR spectra as described above, and the continuous curves are multiexponential fits as in eq 3. It is clear from the initial inspection of the CLS data for the A_1 and A_3 substates that the homogeneous component for A_3 is larger. This is manifested in the smaller deviation of the initial value of A_1 CLS data from unity as compared with that of A_3.

The data in Figure 4 end at 40 ps when both curves have decayed to ~0.2. The data can be fit with or without a static term (see eq 3). The CLS data were fit with a biexponential function with and without an offset (static term). In the fits that included an adjustable offset, the fits converged with an offset of zero. Therefore, the fits shown in Figure 4 do not include an offset. The data for wild type MbCO are taken on samples with higher concentration than the double mutant because there is less tendency of the wild type protein to aggregate at high concentration. The result was that the wild type data could be acquired to 80 ps. At 80 ps, the value of the CLS has dropped to 0.09. Fitting this data with and without an offset showed that the offset could be at most a few percent. In addition, the simulated FFCFs discussed below, which run to 100 ps, could

(79) Finkelstein, I. J.; Zheng, J. R.; Ishikawa, H.; Kim, S.; Kwak, K.; Fayer, M. D. *Phys. Chem. Chem. Phys.* **2007**, *9*, 1533.

(80) Asbury, J. B.; Steinel, T.; Kwak, K.; Corcelli, S. A.; Lawrence, C. P.; Skinner, J. L.; Fayer, M. D. *J. Chem. Phys.* **2004**, *121*, 12431.

(81) Woutersen, S.; Pfister, R.; Hamm, P.; Mu, Y. G.; Kosov, D. S.; Stock, G. *J. Chem. Phys.* **2002**, *117*, 6833.

(82) Finkelstein, I. J.; Ishikawa, H.; Kim, S.; Massari, A. M.; Fayer, M. D. *Proc. Natl. Acad. Sci. U.S.A.* **2007**, *104*, 2637.

(83) Massari, A. M.; Finkelstein, I. J.; Fayer, M. D. *J. Am. Chem. Soc.* **2006**, *128*, 3990.

(84) Ishikawa, H.; Finkelstein, I. j.; Kim, S.; Kwak, K.; Chung, J. K.; Wakasugi, K.; Massari, A. M.; Fayer, M. D. *Proc. Natl. Acad. Sci. U.S.A.* **2007**, *104*, 16116.

(85) Ishikawa, H.; Kim, S.; Kwak, K.; Wakasugi, K.; Fayer, M. D. *Proc. Natl. Acad. Sci. U.S.A.* **2007**, *104*, 19309.

(86) Kim, S.; Chung, J. K.; Kwak, K.; Bowman, S. E. J.; Bren, K. L.; Bagchi, B.; Fayer, M. D. *J. Phys. Chem. B* **2008**, *112*, 10054.
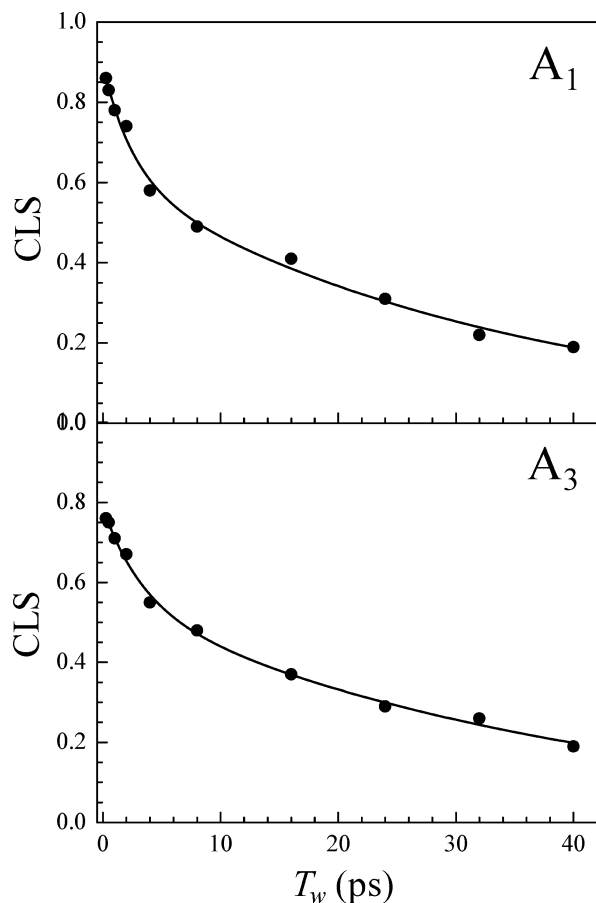
Figure 4. T_w dependent CLS for A_1 and A_3 conformational substates of Mb T67R/S92D. The circles are the data and the curves are biexponential fits. The difference from 1 at $T_w = 0$ is related to the homogeneous line width.

be fit with and without an offset. Again, good fits to the simulated FFCFs were obtained with a multiexponential form. When an offset is included it is less than several percent.

An offset, corresponding to the static term in the FFCF, would reflect structural fluctuations that are too slow to contribute to the data obtained within the experimental time window of 40 ps for the double mutant. Fluctuations out to several times the experimental window contribute to the dynamics.[87] Therefore, the experimental and simulated results suggest that fluctuations that are slower than about a hundred picoseconds comprise at most a few percent of the dynamic sampling of all protein structures that give rise to the double mutant MbCO absorption lines.

The CO inhomogeneously broadened absorption lines and the structural dynamics that cause the observed spectral diffusion are not only local, but rather have contributions from the entire protein.[63] For example, neuroglobin (Nb) is a heme protein with its heme pocket virtually identical to that of Mb. Nb contains a disulfide bond. In spite of the fact that the heme pockets are the same, 2D IR vibrational echoes reveal that the dephasing is quite different in the two systems.[84] In addition, when the Nb disulfide bond, which is ~20 Å from the CO bound at the active site, is severed, the dynamics that are reported by the CO change.[85] The CLS data in Figure 4 show that most of the

(87) Bai, Y. S.; Fayer, M. D. *Phys. Rev. B* **1989**, *39*, 11066.

Table 1. FFCF Parameters from 2D IR Vibrational Echo Experiments and MD Simulations

method	protein	T_2^*(ps)	Γ (cm^{-1})	Δ_1 (cm^{-1})	τ_1 (ps)	Δ_2 (cm^{-1})	τ_2 (ps)
Exp.	Mut.-A_1	7.3	1.4	2.7 ± 0.4	2.5 ± 0.9	4.1 ± 0.2	34 ± 4
Sim.	Mut.-A_1	4.1	2.6	3.2 ± 0.5	8.5 ± 1.0	2.7 ± 0.2	73 ± 11
Exp.	Mut.-A_3	4.6	2.3	2.6 ± 0.4	3.3 ± 1.0	3.9 ± 0.2	39 ± 4
Sim.	Mut-A_3	2.7	4.0	3.4 ± 0.3	4.9 ± 0.7	3.4 ± 0.2	62 ± 6
Exp.	wt -A_1	5	2.1	2.2 ± 0.5	4 ± 1.0	3.2 ± 0.4	32 ± 4
Sim.	wt-A_1	4	2.6	2.3 ± 0.3	3 ± 0.8	2.5 ± 0.2	42 ± 4

structural dynamics of the myoglobin double mutant that couple to the CO stretch occur on fast (<100 ps) and ultrafast time scales.

The FFCF parameters for the T67R/S92D Mb double mutant and wild type Mb are given in Table 1. Because any static contribution to the FFCF is at most a few percent, and excellent fits are obtained without the additional adjustable parameter, we report the results of fits with no static component. (If a static component is included, all of the time constants become ~30% shorter.) For the double mutant, the motionally narrowed term T_2^* is almost a factor of 1.5 shorter for A_3 than A_1. The A_1 substate has a fast (2.5 ps) decay followed by a slower decay of 34 ps. The A_3 band has a 3.3 ps decay followed by a slower decay of 39 ps. Except for the homogeneous component, the dynamics of these two substates are very similar. For wild type MbCO in the A_1 substate, the homogeneous pure dephasing time T_2^* is shorter than that of the A_1 state of the double mutant. The fast decay time of $\tau_1 = 4$ ps is somewhat longer than that of the A_1 state of the double mutant. The slowest decay time of $\tau_2 = 32$ ps is essentially identical to that of the double mutant, 34 ps. Overall, the double mutant, in which one amino acid in the pocket and one near the pocket are changed, does not have structural dynamics that are profoundly different from those of wild type MbCO. This is in contrast to the single mutant, H64V, in which the distal histidine is replaced with a valine.[62] Removing the distal histidine whose motions are strongly coupled to the CO stretch results in a large reduction of the dynamics observed in the 100 ps experimental time window. There are significant differences between the double mutant and wild type MbCO, which are manifested in the change in absorption spectrum and the appearance of chemical exchange between the A_1 and A_3 substates. The similarities and differences between the double mutant and wild type MbCO will be discussed further below.

C. Molecular Dynamics Simulation. Representative trajectories of fluctuations in the CO vibrational frequency of the T67R/S92D MbCO double mutant computed from molecular dynamics trajectories and eq 1 are shown in Figure 5. In Figure 5A, the CO partial charges are set to gas phase values[45,70] $q = \pm 0.021e$, and in Figure 5B, these charges have the value[65] $q = \pm 0.17e$. Each trajectory shows clear two-state dynamics, similar to those obtained previously in simulations of wild-type Mb.[9] We interpret the state with $\delta\omega > 0$ as the A_1 spectroscopic substate and the state with $\delta\omega < 0$ as the A_3 substate, as in wild-type Mb.[9] The structures of these states differ primarily in the orientation of the imidazole ring on the distal histidine His 64. In the A_3 state, the $N_\varepsilon - H$ bond on this imidazole is pointing toward the CO, while in the A_1 state, the imidazole is reoriented to produce a weaker interaction with the CO.[9] We are not able to discern any significant difference between these structures for T67R/S92D and their analogs for wild-type Mb. For the smaller CO partial charges used in Figure 5A, the reorientation of the imidazole group of His 64 (exchange between the A_1 and A_3 substates) occurs at a higher rate than
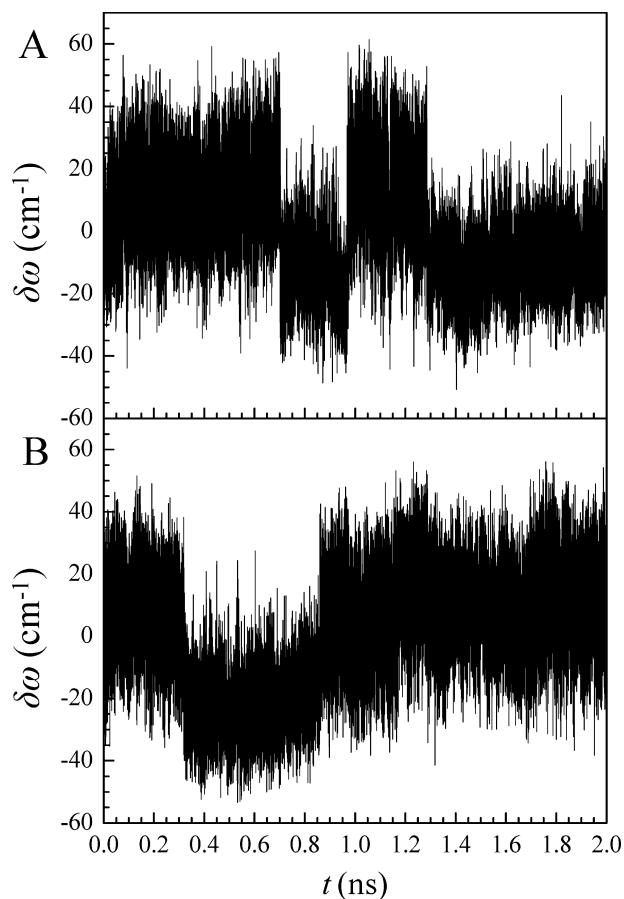
Figure 5. Fluctuating vibrational frequency of CO bound to T67R/S92D mutant Mb is shown for a molecular dynamics trajectory with partial charges on the CO of (A) the gas phase values $q = \pm 0.021e$, and (B), $q = \pm 0.17e$.
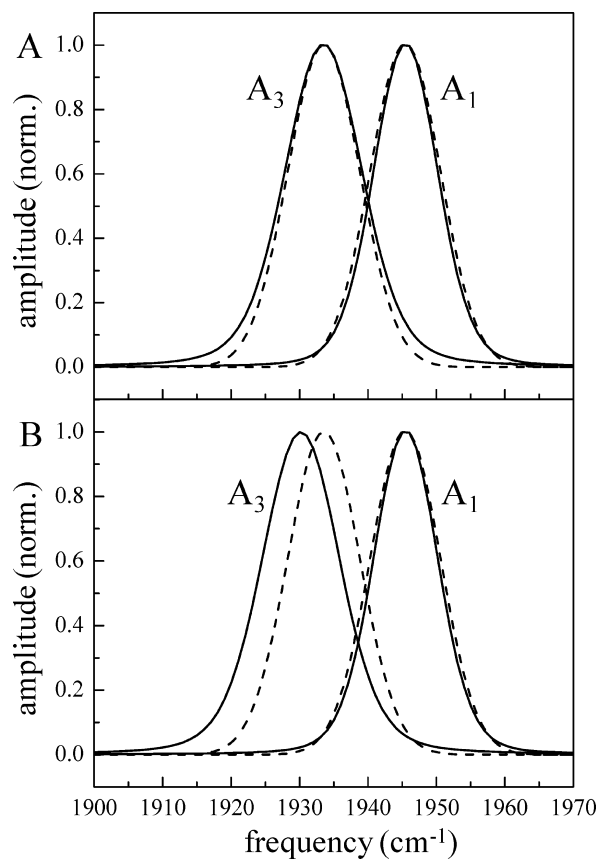

Figure 6. Linear absorption spectra (normalized) of the A_3 and A_1 states of T67R/S92D mutant Mb calculated from MD simulations (solid curves) are compared to the experimental spectra (dashed curves). (A) To compare line shapes, the peak frequencies of the simulated peaks are aligned with those of the experimental spectra. A single adjustable parameter is used to simultaneously fit both bands (see text). (B) Peak frequency of the simulated A_3 spectrum relative to A_1 is determined from simulation.

for the case of the larger CO partial charges used in Figure 5B. However the FFCFs for each substate were not significantly sensitive to these partial charges. In these calculations, the CO partial charges affect the dynamics of switching between states, but do not significantly affect the dynamical fluctuations within each state. Because of the sensitivity of state switching dynamics to CO partial charges and in the absence of optimized values for these charges in this mutant Mb, we do not present calculated exchange rates between A_1 and A_3 substates from these simulations.

D. Comparison of the Experimental and Simulation Results. Linear lineshapes calculated from simulated frequency auto-correlation functions for the A_1 and A_3 lines (solid curves) are shown in Figure 6A, where they are compared to lineshapes fit to the experimental absorption spectrum (dashed curves) as shown in Figure 2. The simulations yield line shapes and the frequency shift between the two bands, but do not provide absolute frequencies. Since we do not calculate exchange rates between A_1 and A_3 states for the reasons given previously, we also do not determine relative peak amplitudes. The bands are normalized, and the center frequencies of the simulated spectra are aligned with the experimental values to facilitate comparison of line shapes. The coupling parameter λ in eq 1 was adjusted to give the best simultaneous fit to both line shapes. This is the only adjustable parameter used to relate simulation results to experimental data. From these line shape fits, $\lambda = 1.0$ cm^{-1}/(MV/cm). As can be seen in Figure 6A, the simulated FFCFs together with this value of λ reproduce the experimental line shapes well.

This value of λ is then used below in calculations of nonlinear spectra. The capacity of the simulations to reproduce the frequency shift between A_1 and A_3 is assessed in Figure 6B, which differs from Figure 6A only in that the peak frequency of the simulated A_3 line is determined from the simulated frequency shift between A_1 and A_3. As can be seen from Figure 6B, the shift is underestimated by $\sim$4 cm^{-1}.

The FFCFs obtained directly from MD simulations for both A_1 and A_3 are shown in the insets in Figure 7. The first rapid decays, which are complete in a few hundred femtoseconds, are followed by much slower time evolutions. The initial fast decays give rise to the homogeneous component of both the linear absorption spectra and the 2D IR spectra. It is not possible to directly compare simulated FFCFs with the experimentally derived CLS decays in Figure 4, because the CLS plots do not include decays in the homogeneous or motionally narrowed limit as discussed in Section IIB. To compare the simulation and 2D IR experimental results, vibrational echo spectra at different waiting times were calculated from the FFCFs obtained from MD simulations that are shown as insets in Figure 7. T_w dependent CLS analysis was performed on the calculated spectra using the same procedure that generated the CLS plots in Figure 4 from measured spectra. Combining the CLS analysis of simulated 2D spectra with the simulated absorption spectra, simulated CLS decays were obtained for the A_1 and A_3 substates, and are shown by the solid curves in Figure 7. The experimental CLS decays in Figure 4 are reproduced by the dashed curves
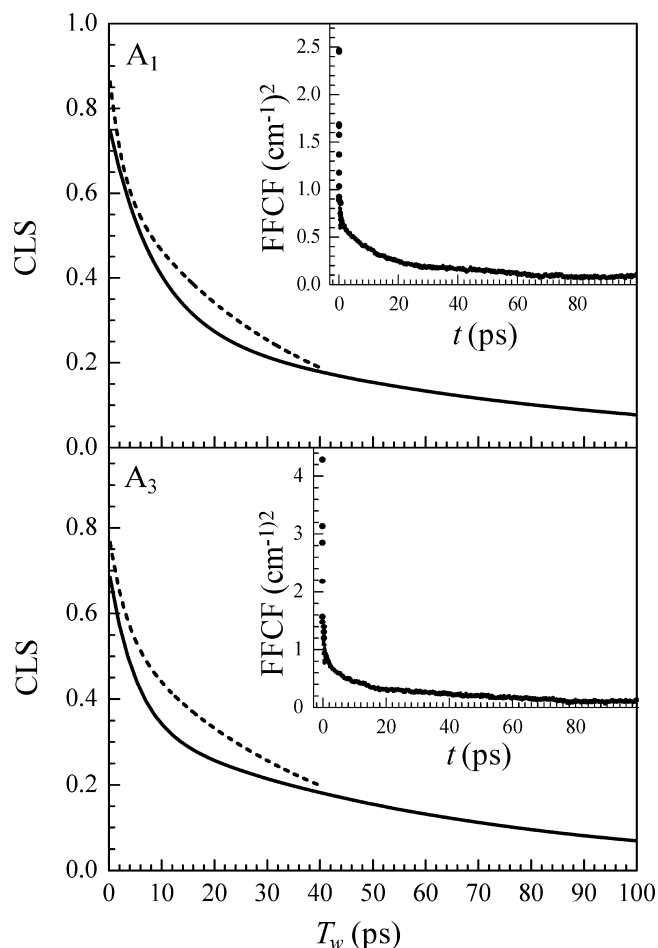
Figure 7. Simulated FFCFs (insets) and simulated and experimental CLS for the A_1 substate (top panel) and the A_3 substate (bottom panel) of the T67R/S92D double mutant of MbCO. In the main parts of the panels, the solid curves are the CLS obtained from the MD simulations and the dashed curves reproduced from Figure 4 are obtained from experiment.

in Figure 7. At 100 ps, the simulated CLS have decayed to ~6% and are still decaying. The small value of the CLS at 100 ps suggests that there is no very slow component of the structural fluctuations within a substate that are not reflected in the FFCF. If there is a very slow component, its amplitude is very small.

The FFCF parameters of simulated T67R/S92D double mutant and wild type Mb are given in Table 1. The multiexponential fits to the simulated CLS decays for both the A_1 and A_3 substates did not include a static component. Like the experimental data, it is possible to fit the simulated CLS with a static component, but it is very small. Table 1 shows that simulated time scales are generally slower than the experimental results, but within a factor of 2 of them, and that simulated root-mean-squared frequency fluctuations, Δ_1 and Δ_2, are generally of the correct magnitude. Simulations agree with experiment, for example, in predicting that the motionally narrowed dephasing time T_2^* is shorter for the A_3 substate of the mutant than for the A_1 substates of the mutant and the wild type protein. The simulations also correctly show that both Δ_1 and Δ_2 for the wild-type Mb are smaller than those for either substate of the mutant. The simulations do not however reproduce the trends in time scales t_1 and t_2 for the A_1 and A_3 substates of the mutant. The differences among the experimental parameters in Table 1 for the A_1 and A_3 substates of the mutant protein and the A_1 substate of the wild-type Mb are not large,

but the trends are not consistently reproduced by the simulation. It should be noted that the only adjustable parameter in comparing simulation to experiment is λ, whose value is chosen from the comparison of linear absorption line shapes in Figure 6A. Since the effect of varying λ is to scale the amplitude of the FFCFs in the inset of Figure 7, the CLS decays in Figure 7 are approximately independent of λ. The agreement between solid and dashed curves in Figure 7 indicates that the simulations generally capture the amplitudes and time scales of the protein dynamics that couple to the CO vibration. The simulations also show the similarities between the spectroscopy of the T67R/S92D mutant and wild type Mb. However, the most significant shortcoming of the simulations is not one of the relatively minor discrepancies shown in Table 1 but rather that the simulations do not provide quantitative predictions for the switching times between the substates nor for the relative populations of these two states.

Our computations are based on one of a family of models in which the vibrational frequency of a chromophore is assigned a time-dependence driven by classical motions of surrounding degrees of freedom.[88–90] Here, the relation between vibrational frequency and classical dynamics is given by eq 1. The absorption and 2D IR spectra are then calculated from standard approximations,[9] based on weak coupling between the chromophore and its environment, that connect observables to the FFCF. Discrepancies between calculation and measurement may in principle be ascribed to the breakdown of any assumptions underlying this treatment or to deficiencies in the force field used to describe the protein dynamics. As shown in Figure 5, the switching time between A_1 and A_3 states is sensitive to the partial charges assigned to CO, although the dynamics within each substate are not. The CO chromophore in myoglobin is a high frequency vibration coupled to lower frequency protein and solvent dynamics, so that the assumptions underlying the connection between FFCF and spectroscopic observables are reasonable. If these assumptions are accepted, the comparison of MD results to 2D IR spectra represents a test of the capacity of a force field, typically developed to satisfy structural or thermodynamic criteria, to reproduce dynamics and relaxation on the experimental time scale.

The Amber force field used here reproduces the experimental dynamics within each spectroscopic substate to a reasonable degree, and suggests that this force field provides a plausible description of the motions of wild-type and T67R/S92D mutant MbCO on the time scale of tens of ps. The agreement between calculation and measurement is sufficient that the simulations may be used at least qualitatively to interpret the measured spectra, providing, for example, structural assignments for the spectroscopic substates. The primary significance of this comparison is not, however, the outcome of assessing one particular force field, but rather the procedure of applying vibrational echo measurements to test the dynamical accuracy of a force field. Our comparison of calculated and measured spectra also exposes specific deficiencies in the capacity of this force field to describe the dynamics of heme proteins. The shortcomings and virtues of different versions of Amber force fields, including the ff03 used here,[60] in reproducing minimum energy structures of proteins have been described.[54] We have performed preliminary calculations[66] of vibrational echoes for wild-type Mb and for

(88) Kwac, K.; Lee, H.; Cho, M. H. *J. Chem. Phys.* **2004**, *120*, 1477.
(89) Jansen, T. L.; Hayashi, T.; Zhuang, W.; Mukamel, S. *J. Chem. Phys.* **2005**, *123*.
(90) Auer, B. M.; Skinner, J. L. *J. Chem. Phys.* **2008**, *129*.

the mutant H64V using the Amber force field ff99SB, which has been shown to be more accurate than other versions in certain applications.[54] These preliminary results for the wild type protein and for H64V suggest that this force field does not provide a significantly different description of the dynamics of fast structural fluctuations in Mb relative to either ff03 or the MOIL force field[91] used by us in previous studies.[53,71] Reproducing the changes in equilibrium populations and exchange rates of the A_1 and A_3 states caused by the two mutations in T67R/S92D poses a challenge for empirical force fields.

IV. Concluding Remarks

Ultrafast 2D-IR vibrational echo experiments and molecular dynamics simulations have independently established the time scales and relative magnitudes of the equilibrium structural fluctuations of the two substates A_1 and A_3 of the myoglobin double mutant T67R/S92D by observing the vibrational dephasing dynamics of the CO stretching mode bound at the heme active site. The time scales and amplitudes of vibrational frequency fluctuations obtained by simulation are in relatively good agreement with results measured in 2D IR experiments, suggesting that the simulations capture those protein dynamics coupled to the CO vibration. The vibrational dynamics of both the substates have an ultrafast decay that gives rise to a motionally narrowed component followed by a fast decay component and a slower component. The experiments and simulations suggest that most of the spectroscopically relevant configurations within the protein substates are sampled in a few hundred picoseconds. A comparative study of the A_1 band of the double mutant with that of wild type myoglobin shows that the structural dynamics of the wild type are somewhat faster than those of the double mutant variant.

A folded protein in a particular substate occupies a minimum on the free energy landscape. However the energy landscape is rough and broad around the minimum, being composed of many local minima separated by low barriers. Transitions from one local minimum to another result in structural fluctuations that produce the spectral diffusion measured by the 2D IR vibrational echo experiments and are reproduced by the molecular dynamics simulations. For both the substates of the double mutant and the A_1 substate of the wild type Mb, virtually all of the configurations corresponding to the different local minima of the free energy surface are sampled within a few hundred picoseconds. The MD simulations do not reproduce the $A_1 - A_3$ substate switching observed in the experiments (see Figure 3). Jumps between the substates are observed in the simulations (see Figure 5). However, the time scale for substate switching

(91) Elber, R.; Roitberg, A.; Simmerling, C.; Goldstein, R.; Li, H.; Verkhivker, G.; Keasar, C.; Zhang, J.; Ulitsky, A. *Comput. Phys. Commun.* **1995**, *91*, 159.

obtained from the simulations is significantly too slow. The simulations do a good job of capturing the structural fluctuations that occur about the local substate minima, but evidently, the simulations do not describe transitions over higher barriers that separate substates well.

The double mutant shows enzymatic activity[48,49] while wild type Mb does not. One of the notable results of this study is that the dynamics of the double mutant and wild type MbCO are very similar. The slowest component of the wild type spectral diffusion has a very similar time scale to that of the double mutant, 32 ps vs 34 ps, which is within experimental error. However, there are differences. In the wild type protein the A_1 substate is the major component, while in the double mutant the A_3 substate predominates. This demonstrates that the potential surface is changed by the double mutation, and the mutations lower the free energy of the A_3 state relative to the A_1 state. In addition, conformation switching between the A_1 and A_3 states is evident in the double mutant (see Figure 3), but is undetectable in the wild type protein. Substate switching is much slower for wild type, too slow to be observed during the experimental time window. The observation of switching for the mutant but not for wild type means that the barrier height separating the A_1 and A_3 substates has been lowered by the double mutation.

From the similarities in the structural dynamics between the double mutant and wild type MbCO, it is clear that the enzymatic activity of the double mutant does not arise from substantial changes in dynamics in a particular substate that might be involved in reaching the transition state for enzymatic reactions. Rather, changes in structure that allow substrate binding and possibly changes in barriers to facilitate conformational accommodation of reactants and products are the cause of the increased enzymatic activity of the double mutant. Experiments are currently in progress to examine the dynamics of the double mutant with a substrate bound in the enzymatic pocket.

Supporting Information Available: Complete author list for ref 58. This material is available free of charge via the Internet at http://pubs.acs.org.

JA108491T